Degradation Mechanism of Tris(2-Chloroethyl) Phosphate (TCEP) as an Emerging Contaminant in Advanced Oxidation Processes: a DFT Modelling Approach

Hui Xia, Wenjing Zhang, Yuesuo Yang, Diane Purchase, Chuanqi Zhao, Xiaoming Song, Yuanyuan Wang

Graphical Abstract
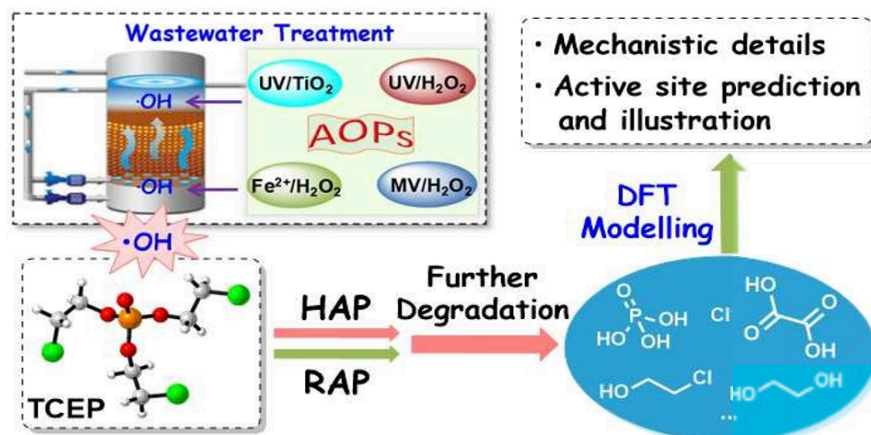
Highlights:

✓ Mechanistic details of TCEP degradation in AOPs was investigated by DFT method.

✓ Reactivity sites of TCEP were revealed by the BDE and DIE analysis.

✓ Potential degradation pathways of TCEP were demonstrated by DFT modelling.

✓ Gibbs free energy profiles for each transformation were clearly presented.

✓ Common degradation products in AOPs on ·OH were identified.

Degradation Mechanism of Tris(2-Chloroethyl) Phosphate (TCEP) as an Emerging Contaminant in Advanced Oxidation Processes: a DFT Modelling Approach

Hui Xia[a], Wenjing Zhang[b*], Yuesuo Yang[a,c*], Diane Purchase[d], Chuanqi Zhao[a],

Xiaoming Song[a], Yuanyuan Wang[c]

[a] Key Laboratory of Regional Environmental and Eco-restoration (Shenyang University), Ministry of Education, Shenyang 110044, China
[b] College of Chemistry, and Institute of Green Catalysis, Zhengzhou University, Zhengzhou 450001 China
[c] Key Laboratory of Groundwater Environmental and Resources (Jilin University), Ministry of Education, Changchun 130021, China
[d] Department of Natural Sciences, Middlesex University, The Burroughs, London NW4 4BT, UK

Abstract

As a typical toxic organophosphate and emerging contaminant, tris(2-chloroethyl) phosphate (TCEP) is resistant to conventional water treatment processes. Studies on advanced oxidation processes (AOPs) to degrade TCEP have received increasing attention, but the detailed mechanism is not yet fully understood. This study investigated the mechanistic details of TCEP degradation promoted by ·OH using the density functional theory (DFT) method. Our results demonstrated that in the initial step, energy barriers of the hydrogen abstraction pathways were no more than 7 kcal/mol. Cleavage of the P-O or C-Cl bond was verified to be possible to occur, whilst the C-O or C-C cleavage had to overcome an energy barrier above 50 kcal/mol, which was too high for mild experimental conditions. The bond dissociation energy (BDE) combined with the distortion/interaction energy (DIE) analysis disclosed origin of the various reactivities of each site of TCEP. The systematic calculations on the transformation of products generated in the initial step showed remarkable exothermic property. The systematic calculations on the transformation of products generated in the initial step showed remarkable exothermic property. The novel information at molecular level provides insight on how these products are generated and offers valuable theoretical guidance to help develop more effective AOPs to degrade TCEP or other emerging environmental contaminant.

Keywords: TCEP, degradation mechanism, hydroxyl radical, DFT, advanced 12 oxidation processes

* Corresponding authors: yangyuesuo@jlu.edu.cn (Y. Yang); zhangwj@zzu.edu.cn (W. Zhang)

1. Introduction

Due to increasingly stringent safety and environmental regulations and the relatively low cost of production, polybrominated biphenyl ethers flame retardants have gradually been phased-out worldwide and replaced by organophosphate flame retardants (OFRs) (Chen and Bester 2009, Li et al. 2017). Tris(2-chloroethyl) phosphate (TCEP) is one of the most common OFRs. It is used as an annexing agent in industrial products, such as building materials, automobile components, paint, film, shoes, tires and so on, to enhance their fire resistance and thermostability (Kim et al. 2017, Liu et al. 2020, Pantelaki and Voutsa 2019, Reemtsma et al. 2008, Wei et al. 2015). However, recent study (Yang et al. 2018a) demonstrated that TCEP could cause intestinal damage, DNA damage, oxidative stress and other abnormal activity changes in earthworms, and exert stronger toxicity than tricresyl phosphate (TCP) under the same concentrations. TCEP also exhibited neurotoxicity in mammals and interfered with normal physiological and biochemical processes in rats (Yang et al. 2018b). Humans are exposed to TCEP through inhalation, inadvertent ingestion or dermal absorption of dust particles (Pang et al. 2019). A number of studies (Follmann and Wober 2006, Hoffman et al. 2017) confirmed TCEP is an endocrine disruptor and carcinogen. TCEP has been widely released into environment in the world (Antonopoulou et al. 2016, Cui et al. 2017, Greaves and Letcher 2017, Ma et al. 2017, Pang et al. 2019, Sorensen et al. 2015). Considerable TCEP has been reported to present in drinking water (Ye et al. 2017), waste water (Greaves and Letcher 2017, Kim et al. 2017), natural groundwater (Antonopoulou et al. 2016, Wolschke et al. 2015) and even human milk (Cechova et al. 2017). Consequently, TCEP has been included in the European Commission second priority list (Kim et al. 2013, Tang et al. 2018) and the candidate list of Substance of Very High Concern for Authorization (ECHA 2010). In order to develop appropriate water and wastewater treatment technology, the toxicology of TCEP and its potential threat to the eco-environment have to be properly understood.

Technically, TCEP, as one category of emerging environmental contaminants (Yang et al. 2019), is completely recalcitrant to the conventional water and wastewater treatment due to its relatively high-water solubility and non-degradability. However, advanced oxidation processes (AOPs), such as UV/TiO$_2$ (Abdullah and O'Shea 2019, Alvarez-Corena et al. 2016, Ye et al. 2017), UV/H$_2$O$_2$ (Liu et al. 2018b), the Fenton processes (Liu et al. 2020, Wu et al. 2018) including microwave (MW) enhanced Fenton process (Du et al. 2018) have been demonstrated to be viable and effective options to attenuate TCEP in a wide concentration range (Miklos et al. 2018, Salimi et al. 2017, Xu et al. 2017). Scientific consensus is that the hydroxyl radical (·OH) is the common key feature of the above mentioned AOPs for TCEP degradation, due to the fact that ·OH is one of the most oxidative radical, second only to the fluorine atom (Miklos et al. 2018, Navalon et al. 2010). This is also found in the decomposition of

most organic compounds (Biard et al. 2018, Ike et al. 2019, Rusevova Crincoli and Huling 2020). The possible routes for ·OH generation in various AOPs were summarized in Table 1. For example, when H_2O_2 in solution of the Fenton reactions was exposed to the MW irradiation, it generated extra ·OH due to the molecular stimulation to high vibrational and rotational energy levels, leading to the enhanced 2 TCEP degradation (Du et al. 2018).

Unfortunately, only limited theoretical investigations on the mechanism of detailed degradation have been reported compare to the extensive technical and applied studies (Li et al. 2017, Li et al. 2018b, Luo et al. 2018, Zhou et al. 2018). Li et al. (Li et al. 2017) investigated the ·OH initiated oxidation of tris(2-chloroisopropyl) phosphate (TCPP), another type of OFR with similar structure to TCEP, but it focused mainly on the atmospheric transformation kinetics and the removal mechanisms of TCPP initiated by ·OH. Density functional theory (DFT) is a widely used mechanical modelling technique in quantum chemistry for investigation of the electronic structures of multiple-component systems with high accuracy and low computational time (da Silva et al. 2020); it is poorly employed in the environmental field so far, but it's believed a robust and powerful tool to understand the in-depth treatment mechanism of pollutants at molecular level. To the best of our knowledge, nothing is reported on the systematic theoretical investigations toward the ·OH initiated degradation of TCEP in water field using the DFT protocol.

However, several studies have been conducted to validate these reactive mechanisms by using the high-resolution experimental analytic techniques, such as GC-MS, HPLC-MS/MS, Q-TOF, NMR spectrometer (Abdullah and O'Shea 2019, Chen et al. 2019b, Du et al. 2018, Liu et al. 2020, Liu et al. 2018b, Wu et al. 2018, Ye et al. 2017). These studies indicated two possible pathways for the initial step of TCEP degradation, namely the hydrogen abstraction initiated pathway (HAP) and the ·OH attack initiated pathway (RAP), as illustrated in Figure 1. There was only limited information available on the mechanistic details so far.

Additional degradation compounds other than the RAP and HAP reaction products 6 can be detected via various techniques as listed in Table 2. Much uncertainty exists in how they are generated and what causes the differences in intensities of the detected intermediates. The DFT protocol has been demonstrated as one of the most efficient methods at the molecular level (Bai et al. 2019a, Bai et al. 2019b, Chen et al. 2019a, Li et al. 2020b, Ran et al. 2016, Zhang et al. 2019); it can provide important information that helps to understand the removal process of emerging contaminants such as TCEP using AOPs and evaluate the toxicology of the intermediates products (Zhang and Zhou 2019, Zhanqi et al. 2007).

Table 1. Possible mechanism for generation of ·OH in various AOPS.

AOPs	Proposed ·OH generation mechanism	References
UV/TiO$_2$	$TiO_2 + h\upsilon \rightarrow e^- + h^+$ $h^+ + H_2O$ $\rightarrow \cdot OH + H^+$ $h^+ + OH^- \rightarrow \cdot OH$ $e^- + O_2 \rightarrow O_2^{\cdot-}$ $O_2^{\cdot-} + H^+ \rightarrow \cdot OOH$ $2 \cdot OOH \rightarrow O_2 + H_2O_2$ $H_2O_2 + O_2^{\cdot-} \rightarrow \cdot OH + OH^- + O_2$	(Ye et al. 2017, Zhanqi et al. 2007)
UV/H$_2$O$_2$	$H_2O_2 + h\upsilon \rightarrow 2\cdot OH$ $\cdot OH + H_2O_2 \rightarrow \cdot OOH + H_2O$ $\cdot OOH + H_2O_2 \rightarrow \cdot OH + H_2O + O_2$ $2\cdot OOH \rightarrow O_2 + H_2O_2$ $\cdot OOH + \cdot OH \rightarrow H_2O + O_2$	(Chen et al. 2019b, Liu et al. 2018a)
Fenton process	$Fe^{2+} + H_2O_2 + H^+ \rightarrow Fe^{3+} + \cdot OH + H_2O$	(Zhang and Zhou 2019)
MW enhanced Fenton process	$MW + H_2O_2 \rightarrow 2\cdot OH + H_2O$	(Du et al. 2018, Miklos et al. 2018)

The electronic structures of chemical species, their transformation details in the chemical reactions and environmental controls in the treatment processes can be quantified in detail using DFT (Ghosh et al. 2018). For example, the active sites on diclofenac molecule that are attacked preferentially by radicals have been correctly predicted based on their high Fukui index. For given reactive conditions, the DFT modelling also helped to explain the preferred degradation pathways of complicated chemical reactions (Liu et al. 2019). As for the hydrogen evolution related to chemical reaction processes caused by the transitional metals doped tungsten phosphide electrocatalysts, the DFT calculations demonstrated that the cobalt dopant simultaneously facilitates the water dissociation, and the hydrogen adsorption processes (Wang et al. 2019). Dzade et al. also reported the structures and properties of the adsorption complexes of As(OH)$_3$ on FeS surfaces by the DFT calculations (Dzade et al. 2017).

Our research group has carried out extensive laboratory and field-based investigations on the degradation of various organic compounds in aqueous environment using dominantly fingerprinting techniques of analytical chemistry (Ahmad et al. 2020, Song et al. 2018, Zhang et al. 2018, Wen et al. 2015, Traverso et al. 2014). These provided a sound foundation for further DFT modelling practice. Previously, DFT has been successful applied to

study catalytic mechanism and selectivity of organic reactions (Bai et al. 2018, Wang et al. 2018). The degradation of TCPP initiated by ·OH revealed by DFT that the HAP mechanism is most favourable as water provided a negative role in the degradation by modifying the stabilities of prereactive complexes via forming hydrogen bonds (Li et al. 2017). The potential reactive sites of 4-chloro-3,5-dimethylphenol (PCMX) in degradation of organophosphate flame retardants were identified based on the DFT calculations, combined with frontier molecular orbital (FMO) and natural population analysis (NPA) analyses (Li et al. 2020). This research aims to provide an understanding of chemical species evolution during the environmental degradation of TCEP during the AOPs. The key objectives are to: (1) investigate the major pathways for the TCEP degradation under AOPs conditions; (2) identify and confirm the two specific processes, the hydrogen abstraction-initiated pathway (HAP) and the ·OH attack-initiated pathway (RAP) of the TCEP degradation; (3) model the possible and 8 potential degradation products of TCEP during the AOPs; and (4) investigate the 9 prospective of using the DFT modelling for the degradation of emerging contaminants 10 in water and wastewater treatment systems.
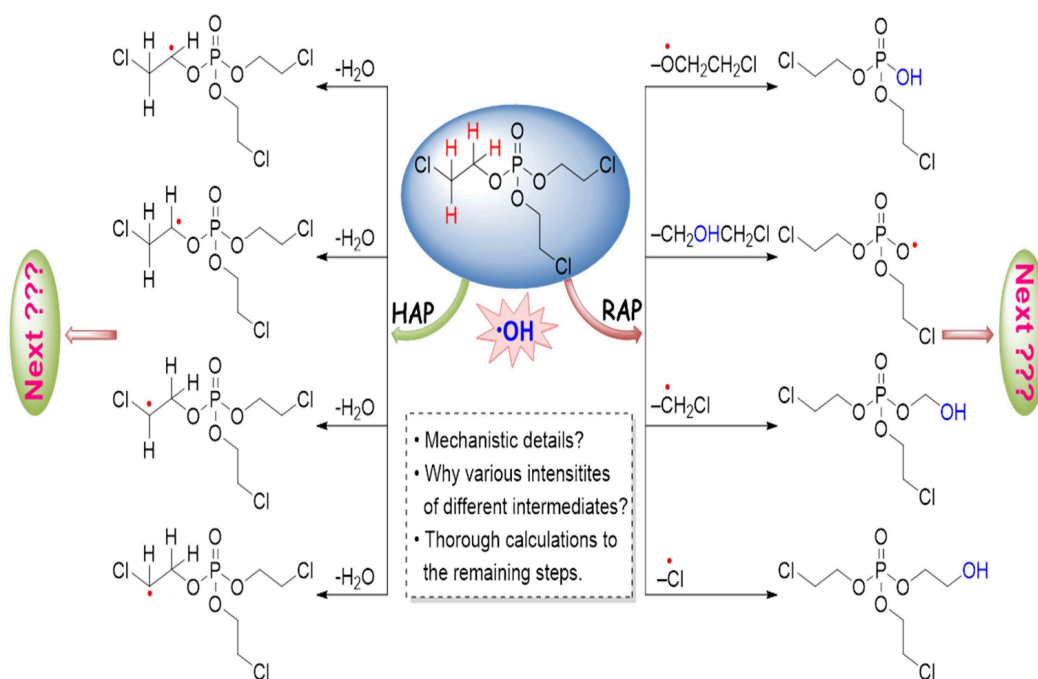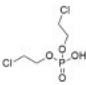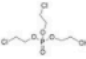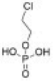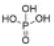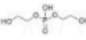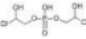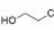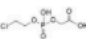

Figure 1. The HAP and RAP mechanism at initial stage of TCEP degradation 3 promoted by the ·OH

Table 2. The experimentally detected intermediates of TCEP degradation in AOPs.

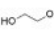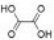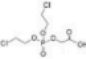| Product[a]	Molecular formula	Molecular weight	Proposed structure	Observed by	Refs.
A (M11)	$C_4H_9Cl_2O_4P$	222.99	*(structure)*	Time-of-Flight HRMS, FT-ICR MS, GC-MS NMR spectrometer	(Abdullah and O'Shea 2019, Chen et al. 2019b, Du et al. 2018, Liu et al. 2020, Liu et al. 2018b, Wu et al. 2018, Ye et al. 2017)
B (M41)	$C_6H_{13}Cl_2O_5P$	267.04	*(structure)*	Time-of-Flight HRMS, FT-ICR MS	(Chen et al. 2019b, Liu et al. 2020, Liu et al. 2018b, Wu et al. 2018, Ye et al. 2017)
C (Ma1)	$C_2H_6ClO_4P$	160.49	*(structure)*	Time-of-Flight HRMS, FT-ICR MS, NMR spectrometer	(Abdullah and O'Shea 2019, Liu et al. 2020, Liu et al. 2018b, Ye et al. 2017)
D (Ma2)	H_3PO_4	98.00	*(structure)*	GC-MS, IC	(Du et al. 2018, Liu et al. 2018b, Ye et al. 2017)
E (Mb2)	$C_4H_8O_6P$	186.03	*(structure)*	FT-ICR MS	(Wu et al. 2018)
F (Mc4)	$C_4H_9Cl_2O_6P$	254.99	*(structure)*	FT-ICR MS	(Wu et al. 2018)
G (Ms1)	C_2H_5ClO	80.51	*(structure)*	GC-MS	(Du et al. 2018, Liu et al. 2020)
H (Ms2)	$C_2H_6O_2$	62.07	*(structure)*	GC-MS	(Du et al. 2018)
I (Ms9)	$C_2H_2O_4$	90.03	*(structure)*	GC-MS	(Du et al. 2018)
J (Mb6')	$C_6H_{11}Cl_2O_6P$	281.03	*(structure)*	FT-ICR MS	(Chen et al. 2019b, Liu et al. 2020, Wu et al. 2018)
K (Mb7')	$C_4H_8ClO_6P$	218.53	*(structure)*	FT-ICR MS	(Wu et al. 2018)
L	Cl^-	36.46	/	IC	(Abdullah and O'Shea 2019, Liu et al. 2020, Liu et al. 2018b, Ye et al. 2017)

a
: Denotation in parentheses represents the one we used in this systematic DFT study.

2. Computational Methodology

2.1. Environmental implication of the TCEP degradation in AOPs

Due to its unique chemical structure, TCEP is not easily degraded and likely to accumulate in the water environment leading to widespread problem for water/wastewater treatment. However, TCEP can be eliminated by strong oxidizing hydroxyl radicals that are widely present in the AOP based technologies. Majority of the research on the degradation of TCEP by AOPs focuses mainly in laboratory macro scale, whereas there is a dearth of information on the reaction sites and pathways of catalytic oxidation by ·OH on molecular level. Based on all above-mentioned experimental results and our research experience, the most widely used quantum chemical DFT method is selected to predict possible pathways of the oxidative degradation of TCEP by hydroxyl radicals. This will provide better understanding of the reactive mechanism of emerging contaminants in water/wastewater treatment.

2.2. DFT modelling protocol

To apply the DFT modelling approach in such an environmental setting at molecular level, follow protocol was adopted. Firstly, data of all the intermediates and products of TCEP degraded by ·OH was collected from the previous data and literature (see Table 2 for more details). Secondly, the reaction sites and possible degradation pathways were proposed according to the experimental results. Finally, the structures of the compounds involved were optimized, and the Gibbs free energy profiles of the speculated degradation pathways were calculated to provide insights into the possible degradation mechanism of TCEP.

2.3. Computational details

All theoretical calculations were carried out using the *Gaussian 09* suit of program (Frisch et al. 2010). The structures of all stationary points involved in this study were optimized using the M06-2X (Zhao and Truhlar 2006) functional and the basis set (Dill and Pople 1975, Hehre et al. 1972), with the solvent effects of the simulated water by the SMD solvation model developed by Truhlar group (Marenich et al. 2009). It should be noted that the computational level of M06-2X/6-311++G(d, p)/SMD$_{water}$ was selected based on following three reasons.

(1) It has been well and widely demonstrated (Bai et al. 2019a, Li et al. 2020a, Wang et al. 2017) that the Minnesota M06-2X functional combined with the triple-ξ split-valence basis set 6-311++G(d, p) works well in predicting rational reaction pathways and correct selectivities of various catalytic reactions. The insight

understanding of origins of various selectivities through various analytical theories at molecular level can be obtained, which is valuable for design of new catalyst with higher efficiency or better selectivity in AOPs.

(2) For degradation of OFRs and other organic pollutants (Li et al. 2017, Li et al. 2018a, Li et al. 2020b, Li et al. 2018b, Li et al. 2020c, Luo et al. 2018, Zhou et al. 2018), there have been a number of DFT studies intending to predict possible mechanisms conducted by using the same or even lower level of computational method. In these studies, theoretical predictions were well demonstrated by experimental technologies, and conversely theoretical explorations provided practical molecular guideline to enhanced and improved AOP technology.

(3) The suitability of the selected computational method was justified by consistent conclusion about the generation order of intermediates produced in the RAP pathway of TCEP degradation with the experimental detection results of the relative intensity variations (Liu et al. 2018b, Ye et al. 2017). Besides, the other two widely used functions, namely CAM-B3LYP (Yanai et al. 2004) and ωB97X-D (Chai and Head-Gordon 2008), also predict the same barrier order for bond cleavage in the initial step of the RAP pathway.

More detailed explanations about the computational level selection can be found in supplementary materials. The frequency calculations were performed at the same level, with the temperature set as 298.15 K and the pressure as 1 atm, to ensure each transition state has one and only one imaginary frequency but others have none. The same level of intrinsic reaction coordinate (IRC) (Gonzalez and Schlegel 1989, Gonzalez and Schlegel 1990) calculations were performed to make sure that each transition state led to the expected reactants and products on the potential energy surface.

The thermal corrections to the Gibbs free energies (G_{corr}) were recalculated using the THERMO program (Fang 2013), free of charge for academic users, to solve the problem of the entropic penalty in thermal corrections based upon the ideal gas-phase model. However, the chemical processes for the thermal correction in water/wastewater are often overestimated (Huang et al. 2010, Liang et al. 2008); therefore, all energies discussed in the present study were calculated by adding the electronic energies calculated by *Gaussian 09* to the G_{corr} so that an improvement to the Fang's atomic radii model can be achieved. Lists of the absolute energies (Table S1) and Cartesian coordinates (Table S2) of all involved structures can be found in supplementary materials.

3. Results and Discussion

This section was organized as follows, (1) computational results and discussion regarding the mechanistic details of the initial degradation step, including the HAP and RAP routes; (2) fundamental principle analyses by

the bond dissociation energy (BDE) and distortion/interaction energy (DIE) analysis for the different activities of each reactive site of TCEP; and (3) a thorough discussion on the proposed mechanism for further transformation of the intermediates generated in the first step, to provide a sound support in unravelling how these detected degradation products listed in Table 2 were yielded.

3.1 The initial step via the HAP and RAP mechanisms.

The abstraction of all the four hydrogen atoms (denoted as H6 to H9 respectively, see Figure 2) in one -OCH$_2$CH$_2$Cl chain was calculated in the HAP process. The energies of TCEP + ·OH were set as the reference of 0.0 kcal/mol, which was also the reference of all other energy profiles in this work. Only the detailed process for H6-abstratction was illustrated as a representation as all abstractions were similar. The calculated results demonstrated the process of absorption of TCEP with the ·OH to give the prereactive complex **M01**, followed by hydrogen transfer from the C3/C4 atom to the ·OH via transition state **TS01**, and finally release of the TCEP radical **M02** and a molecule of water. The theoretically predicted Gibbs energy profiles are given in the lower part of Figure 2. It can be seen that the barriers to abstract the H6-H9 atoms are 6.4, 5.0, 5.0 and 5.4 kcal/mol, respectively, and the product lies 25.4, 24.2, 21.8 and 21.1 kcal/mol below the initial reactants, respectively, indicating a very smooth process and its obvious exothermic feature.
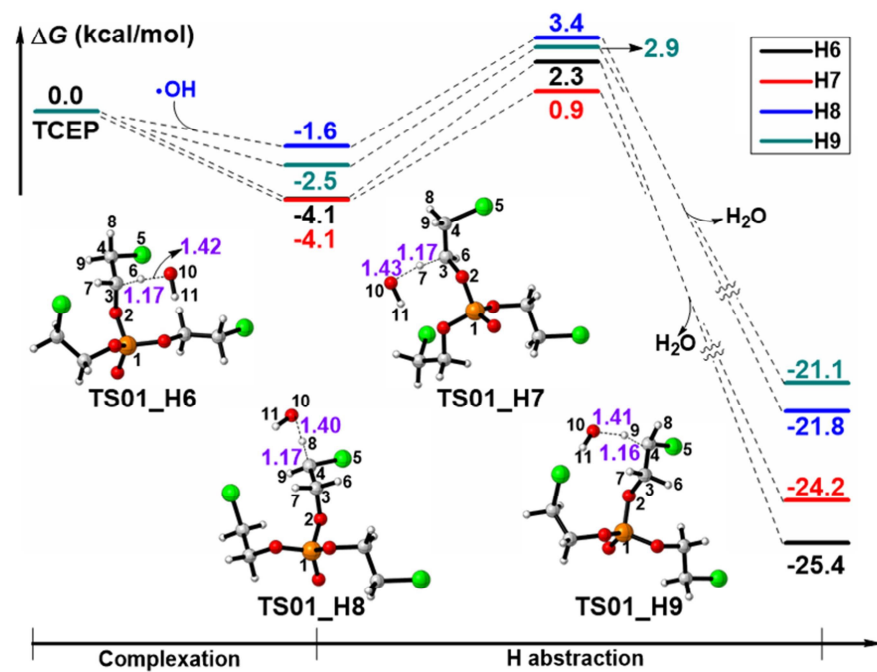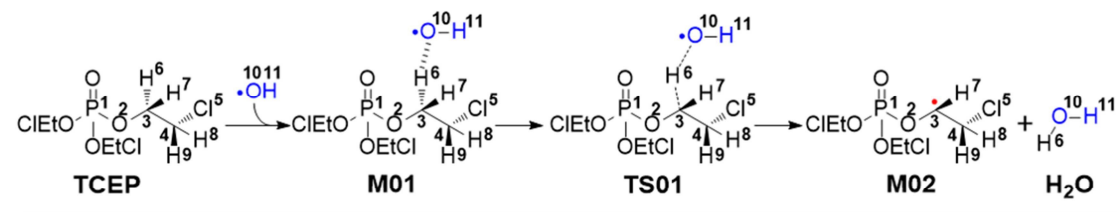
Figure 2. Molecular details of the HAP mechanism (H6 abstraction as the representation), and the Gibbs free energy profiles along with the optimized geometries of all transition states involved. Bond lengths are in angstrom.

With regard to the RAP mechanism, the top key question of concern was to ascertain the most active reaction site. Detailed calculations related to the four pathways were conducted (Figure 3), demonstrated attacking of the ·OH to the P1, C3, and C4 atoms to break the P1-O2, O2-C3, C3-C4, and C4-Cl5 bonds. The pink and blue numbers in parentheses in Figure 3 are barriers predicted by functional ωB97X-D and CAM-B3LYP respectively. The computational results indicated that the reaction to break the P1-O2 or C4-Cl5 bond (via **TS11** or **TS41**, respectively), I was significantly more energetically favorable than that to make the O2-C3 or C3-C4 bonds dissociated to **TS21** or **TS31**, respectively. This is in a good agreement with previous experiments that only the degradation intermediates **M11** and **M41** (denoted as Products A and B in Table 2) were detectd (Liu et al. 2020, Liu et al. 2018b, Ye et al. 2017). Moreover, **M11** was demonstrated to be the intermediate with the highest intensity in the UV-driven ·OH oxidation of TCEP. The lowest barrier and the most stable products via **TS11** provided a theoretical explanation to this experimental observation. The fundamental reason for various reactivities of these four pathways is considered as the different strengths of these four chemical bonds being broken.

The bond dissociation energy (BDE) is the most commonly used thermodynamic quantity to estimate the strength of a organic covalent bond (He et al. 2017, Vleeschouwer et al. 2008). BDE to break the four chemical bonds were calculated through Eq. (1):

$$\text{BDE}(R-R') = E(R\cdot +) \quad E(R'\cdot -) E(\text{TCEP}) \tag{1}$$

where E(R·), E(R'·) and E(TCEP) represent the electronic energies of R radical, R' radical and TCEP, respectively. Noteworthy, here R and R' refer generally to the two groups at ends of the chemical bond of interest, and do not specifically refer to a certain group.

Figure 4 presents the relativity study of the theoretically predicted energy barrier versus BDE. When the reaction goes through **TS21**, **TS31** and **TS41**, the almost linear positive correlation (the Pearson correlation coefficient R equals 0.998) between ΔG and BDE can be clearly demonstrated. However, the situation for **TS11** seems not in line with this correlation (outliner) since the relatively large BDE corresponds to the lowest energy barrier. In order to understand how each chemical bond has been broken and details of the reaction process, the distortion/ interaction energy (DIE) analysis to the four transition states was conducted (Legault et al. 2007). The DIE analysis proposed by Legault et al. is an effective approach to unravel how the reaction barrier comes about (Legault et al. 2007). It has been widely used in mechanism and origin of stereoselectivities studies of various organic and catalytic reactions (Bai et al. 2018, Chai and Head-Gordon 2008, Li et al. 2018b, Wen et al. 2015,

Zhang et al. 2019). The key process was to decompose the activation energy of the concerned transition state into to two main components: the distortion energy ($\Delta E^{\neq}_{dist}$) and interaction energy ($\Delta E^{\neq}_{int}$), as shown in Eq. (2). The former represents the geometric and electronic changes to deform the reactants into their geometry in the transition state, which involves bond stretching, angle decrease or increase, dihedral changes and so on. The latter contains exchange-repulsive and stabilizing electrostatic, polarization, and orbital effects in the structures of transition states. The interaction energy can be recovered as follows:

$$\Delta E^{\neq}_{int} = \Delta - \Delta E^{\neq} E^{\neq}_{dist} \qquad (2)$$

Accordingly, the relative distortion (noted as $\Delta\Delta E^{\neq}_{dist}$) and interaction energy (as $\Delta\Delta E^{\neq}_{int}$) of the four transition states involved in the RAP mechanism were calculated, and all results were listed in Table 3, with corresponding energy of **TS41** set as reference of 0.0 kcal/mol. The results showed that the ·OH did not contribute to the distortion energy, which is reasonable since it possesses a simple structure. The TCEP moiety in **TS11** has the slightest distortion but the most significant interaction compared with that in **TS21** and **TS31**, which indicates that although the P1-O2 bond is very strong (similar BDE with the O2-C3 and C3-C4 bonds), the attack by ·OH could lead to relatively small distortion but strong interactions. In regarding TS41, both the positive and negative items are the smallest (because the reaction occurs at the terminal group), resulting in a relatively low energy barrier. Taking all the above into consideration, the reactivity of breaking the O2-C3, C3-C4, and C4-Cl5 bonds correlated linearly with the bond strength, whilst the synergistic effect of the relatively small distortion and strong interaction facilitated the breaking reaction of the P1-O2 bond to occur, despite of its relatively large BDE.

Table 3. The DIE analysis results to all transition states involved in the RAP mechanisms (Units: kcal/mol)

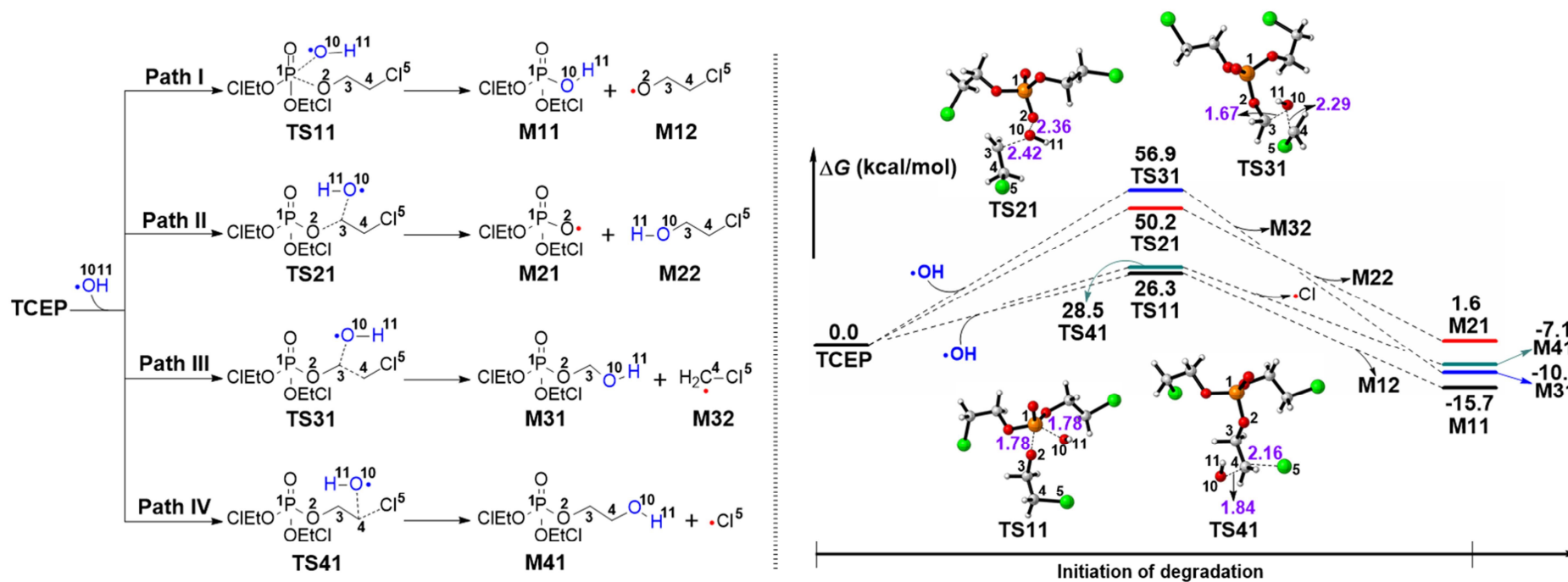| SP	$\Delta\Delta E^{\neq}_{dist}$			$\Delta\Delta E^{\neq}_{int}$
	TCEP	·OH	Total	
TS11	20.5	0.0	20.5	-23.9
TS21	35.8	0.0	35.8	-13.8
TS31	35.7	0.0	35.7	-7.6
TS41	0.0	0.0	0.0	0.0

Figure 3. Potential reaction pathways of the RAP mechanism (*left*), and their corresponding Gibbs free energy profiles along with the optimised geometries of all transition statas involved (*right*). Bond lengths are in angstrom.
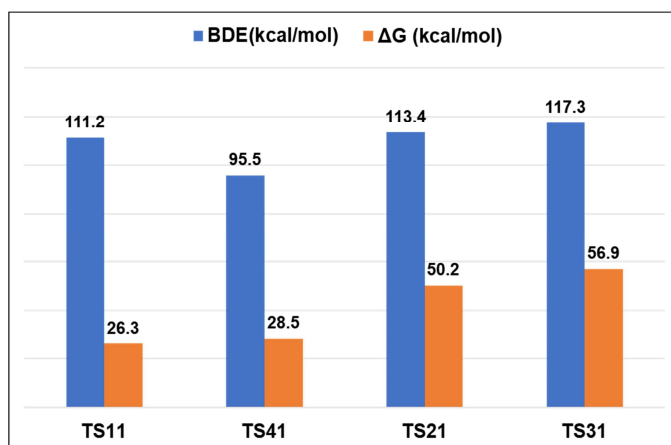
Figure 4. Relativity of the theoretically predicted free energy barrier Δ*G* versus BDEs.

3.2 Further transformation

In addition to the intermediates (Products A and B as listed in Table 2) generated by the RAP reaction, a number of products by further degradation have been reported (Products C to K as listed in Table 2). Detailed computational results on how these products are being generated through Paths I and IV (Figure 3) are presented here. Based upon the systematic molecular calculations, the potential intensive degradation mechanism of TCEP can be achieved, which would support further understanding of the TCEP treatment or even other OFR pollutions by the AOPs technology. Further transformation of the intermediates given through Paths II and III were not considered here because the extremely high energy barrier is required to produce them (ref Figure 4).

3.2.1 **M11**

As shown in the left part of Figure 5, one of the three 2-chloroethoxy groups has been substituted by hydroxyl groups after the initial RAP reaction. The subsequent transformations of M11 should be degradation of the remaining two branches. Based on the computational results of the initial HAP and RAP mechanisms, three possible pathways were proposed, corresponding to the continuous attacks by ·OH to the P1 (Path Ia) atom, the successive attack to the C4'/C4" (Path Ib) atom, and the sequential H9'/H9" (Path Ic) abstraction. It is noteworthy that the products Ma2, Mb2, and Mc4 have been all detected by experimental techniques (Du et al. 2018, Liu et al. 2018b, Wu et al. 2018, Ye et al. 2017), indicating the stable state of these species, with relatively lower Gibbs energy.

The theoretically predicted free energy profiles along with the optimized structures of all involved transition states are presented in the right part of Figure 5. It can be seen that the lengths of the forming (P1-O10) and

breaking (P1-O2' or P1-O2") bonds in **TSa1** and **TSa2** are quite similar. For the Cl radical remove mechanism via **TSb1** and **TSb2**, the lengths of the key bonds (C4'-O10 compared with C4"-O10, and C4'-Cl5' compared with C4"-Cl5") are identical, which should be due to the very limited steric effect difference by one or two 2-chloroethoxy groups since the reaction occurs at the terminal –CH₂Cl group. The results reveal that **TSa1** locates only 0.5 kcal/mol below **TSb1**, and the barriers via **TSa2** and **TSb2** differ by 4.1 kcal/mol, indicating it is more favorable to give the phosphoric acid product **Ma2**.

Regarding the hydrogen abstraction, only the example involving H9' and H9" was calculated as the barriers of all the methylene hydrogen abstraction are quite approximate (Figure 2) and the corresponding product **Mc4** has been detected. The whole process was supposed to proceed through the following steps: absorption of the ·OH to give **Mc1**, H9' abstraction to form a methylene radical **Mc2**, oxidation by another ·OH to give the quenching product **Mc3**, and finally an analogous process to deform the third branch to generate **Mc4**. Similarly, H abstraction (5.1 kcal/mol via **TSc1**) is much more energetically favourable than the ·OH attack (28.0/28.5 kcal/mol via **TSa1**/**TSb1**, respectively), both dynamically and thermodynamically. Moreover, the radical quenching leads to a drastic energy releasing of almost 100 kcal/mol, indicating a significant forward reaction tendency.

Since the hydrogen abstraction was energetically more favourable than the ·OH attack mechanism, it is surprising to detect both **Ma2** and **Mb2** as the products. Actually, one of the aims of this work was to understand the generation mechanism of the degradation products. There is no, as far as we know, experimental demonstration of further reaction of the HAP mechanism, therefore, we would not conduct studies to further processes of the HAP reaction. In regard to reasons that the degradation could not be continued after the HAP initiation, it might be attributed to the following two aspects: (a) It was inadequate to break the stubborn structure of TCEP with only one hydrogen atom being abstracted. Namely, TCEP could not be essentially activated through HAP initiation. In contrast, the S_N2 attack via the RAP reaction directly destroyed the skeleton of TCEP, resulting in its complete activation. (b) As shown in Figure 2, the barrier of reverse reaction of the hydrogen abstraction was around 25 kcal/mol, which was easy to be overcome under experimental conditions of most AOPs. However, due to activation by the initial RAP reaction, the further transformations of the generated intermediates became feasible and were demonstrated to be significantly exothermic processes (Figures 5-7 in following sections), which facilitated the complete degradation of TCEP and inhibits the accumulation of the hydrogen abstraction products (**M02** in Figure 2) from the thermodynamic principle.

3.2.2 **M12**

A possible mechanism for further transformation of the 2-chloroethoxy radical **M12** was proposed, which gives **Ms1**, **Ms2**, and **Ms10** (Products G to I listed in Table 2) as shown in Figure 6.

Firstly, **M12** is reduced by an H_2O molecule, then the given intermediate **Ms1** reacts with the ·OH to release the terminal Cl radical. Subsequently, the glycol **Ms2** is transformed to the 2-hydroxyacetic acid **Ms9** by undergoing successive chemical processes including the H8 abstraction, generation of the ethane triol by radical quenching with the ·OH, triol hydrogen abstraction/1,2-H shift/water remove or H9 abstraction/water remove. Finally, the other alcohol group as in **Ms9** is oxidized to carboxyl group as in **Ms10** by undergoing a similar process (calculations not conducted).

The computational results reveal that the transformation from **M12** to **Ms1** requires energy of 15.3 kcal/mol, which can be overcome easily under mild conditions. The barriers of the subsequent processes of releasing the Cl radical (29.1 kcal/mol) and the H8 abstract (3.9 kcal/mol) have similar magnitudes to that via **TS41** (28.5 kcal/mol in Figure 3) and **TS01** (5.0 kcal/mol in Figure 2), respectively. Then the absorption of an ·OH to quench the radical of **Ms4** results in a significant release of energy of 93.4 kcal/mol. For the activation of **Ms5** by the ·OH, the abstraction of the H9 atom via **TSs5** is shown to be more energetically favorable than the extraction of the hydrogen atom from the triol via **TSs3**. The 1,2-H shift of the H9 atom via **TSs4** requires energy barrier of 24.1 kcal/mol, which is much higher than that via **TSs5**. We conclude that the direct H9 abstraction pathway should be more reasonable for transformation of **Ms5** to **Ms8**. Finally, the **Ms8** radical is stabilized by another molecule of ·OH to furnish the carboxyl acid **Ms9**, with release of energy of more than 100 kcal/mol. The oxalic acid **Ms10** is predicted to locate about 240 kcal/mol lower than **Ms9**, indicating remarkable tendency of the transformation. Our results help to provide better understanding of the possible mechanism in the formation of the degradation products **Ms1**, **Ms2** and **Ms10**.

3.2.3 **M41**

On account of the comparable barrier via TS41 to that via TS11 (Figure 3), 3 possible routes for further transformation of M41 were also proposed, based on the conversion mechanism of Ms2. The whole process is presumed to begin from the H9 abstraction via TSd1, followed by quenching with the ·OH to give the diol Md3 as illustrated in Figure 7. By extracting one of the diol hydrogens or the H8 atom, the intermediate Md6 is formed, which interacts with the ·OH to generate the carboxyl acid Md7. Finally, another ·OH attacks the P1 atom to release a molecule of M12, giving rise to the product Md8. The computational results support the very low barrier of H9 abstraction (3.0 kcal/mol), the energetic favor of the direct H8 abstraction (2.1 kcal/mol) over the successive

hydrogen abstraction/1,2-H shift mechanism (5.3/22.9 kcal/mol, respectively), and the remarkable exothermic property.

3.3 Functional groups in the AOP degradation pathways

Alcohols, aldehydes, ketones, carboxylic acid products were reported as intermediates in extensive studies on the degradation of organic environmental pollutants in AOPs promoted by ·OH (Chen et al. 2019b, Liu et al. 2018c, Luo et al. 2018, Lv et al. 2016, Wang et al. 2020, Xiao et al. 2017). For example, hydroquinone, catechol, resorcinol occurred during the degradation of phenol by ·OH (Lv et al. 2016). According to the DFT study to mechanism of TCEP degradation in AOPs, more insights can be obtained into how these chemical species produced. Specifically, it can be inferred that the H abstraction followed by radical quenching can be a possible pathway to transfer alkyl to alcohol (Figure 8(a)), the successive H abstraction/radical quenching processes can transfer the –CH$_2$ group to aldehyde (Figure 8(b)) or ketone (Figure 8(c)), and the terminal –CH$_3$ group to carboxylic acid (Figure 8(d)). The direct attack of the ·OH to the P center should be a rational pathway to degrade OFRs (Figure 8(e)) when the radical is inadequate. Therefore, the DFT modelling is valuable for getting better understanding to degradation processes of OFRs in AOPs, or even other pollutions promoted by ·OH.

Figure 5. Potential reaction pathways for further transformation of M11 (*left*) and their corresponding Gibbs free energy profiles along with the optimized geometries of all transition states involved (*right*). Bond lengths were in angstrom

Figure 6. The possible reaction pathways for further transformation of **M12** (*left*), and their corresponding Gibbs free energy profiles along with the optimized geometries of

all transition states involved (*right*). Bond lengths are in angstrom.

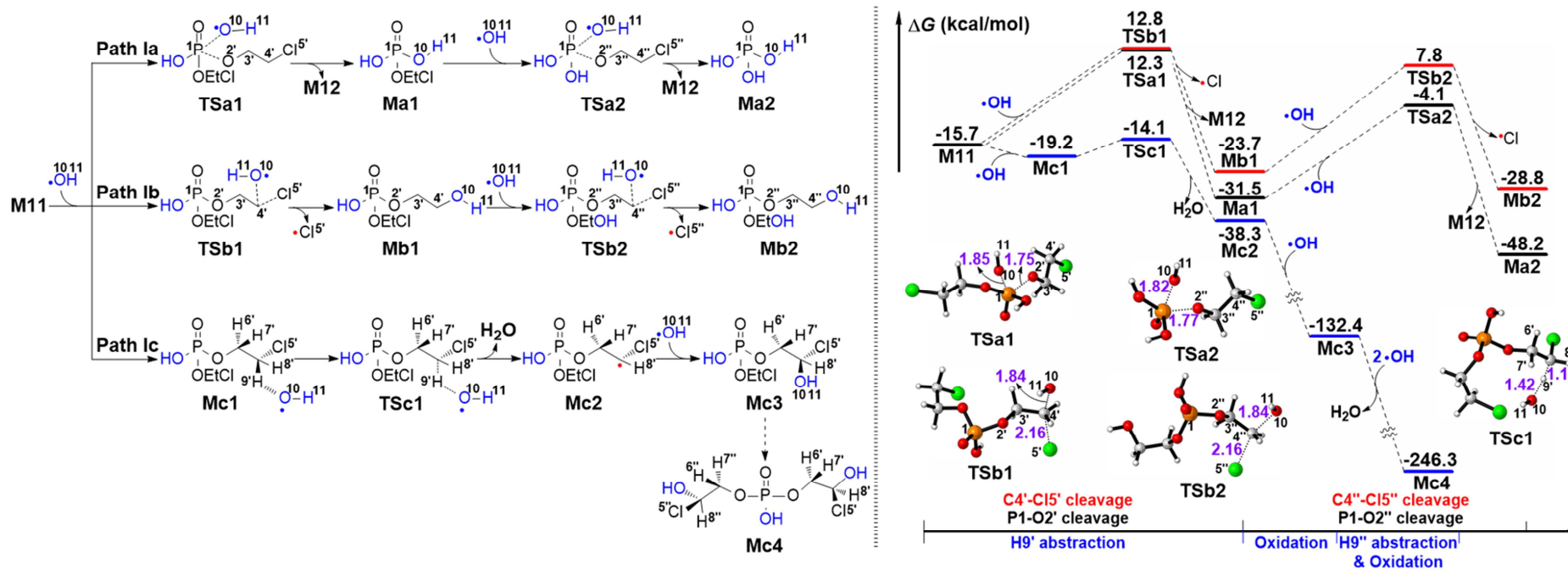**Figure 7.** The possible reaction pathways for further transformation of M41 (*left*), and their corresponding Gibbs free energy profiles along with the optimized geometries of all transition states involved (*right*). Bond lengths are in angstrom.
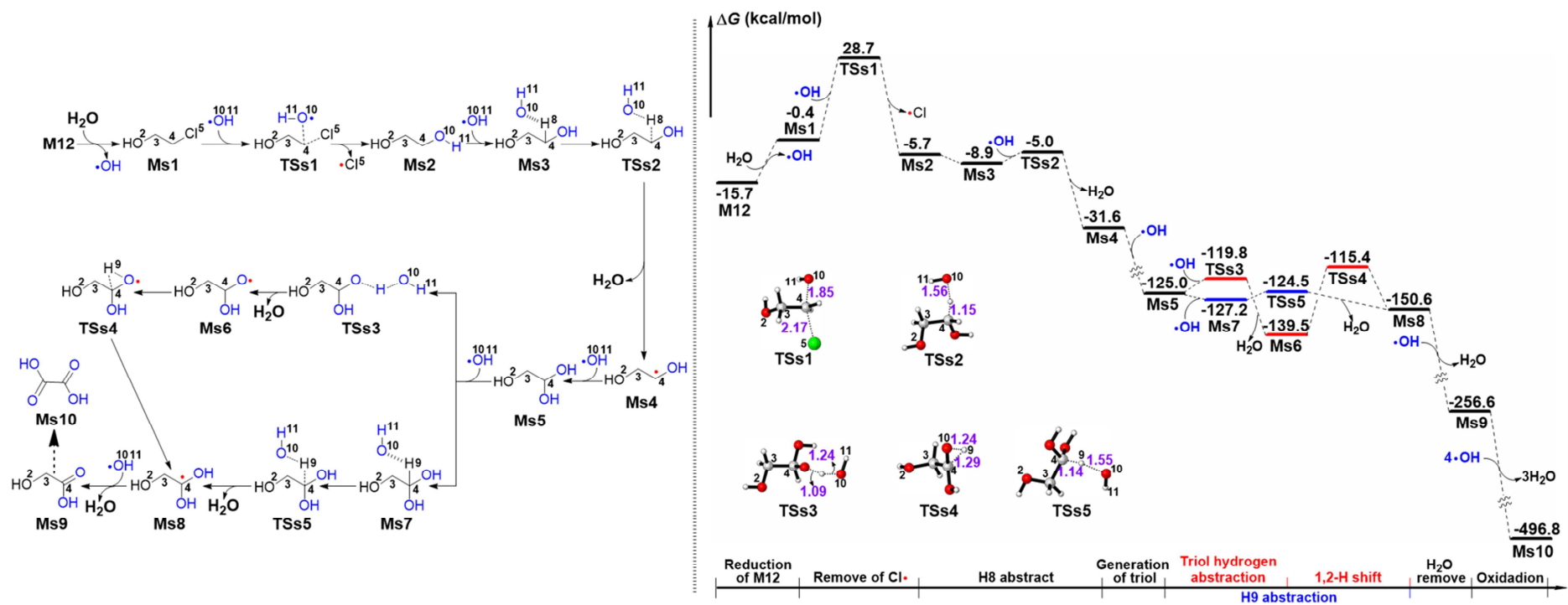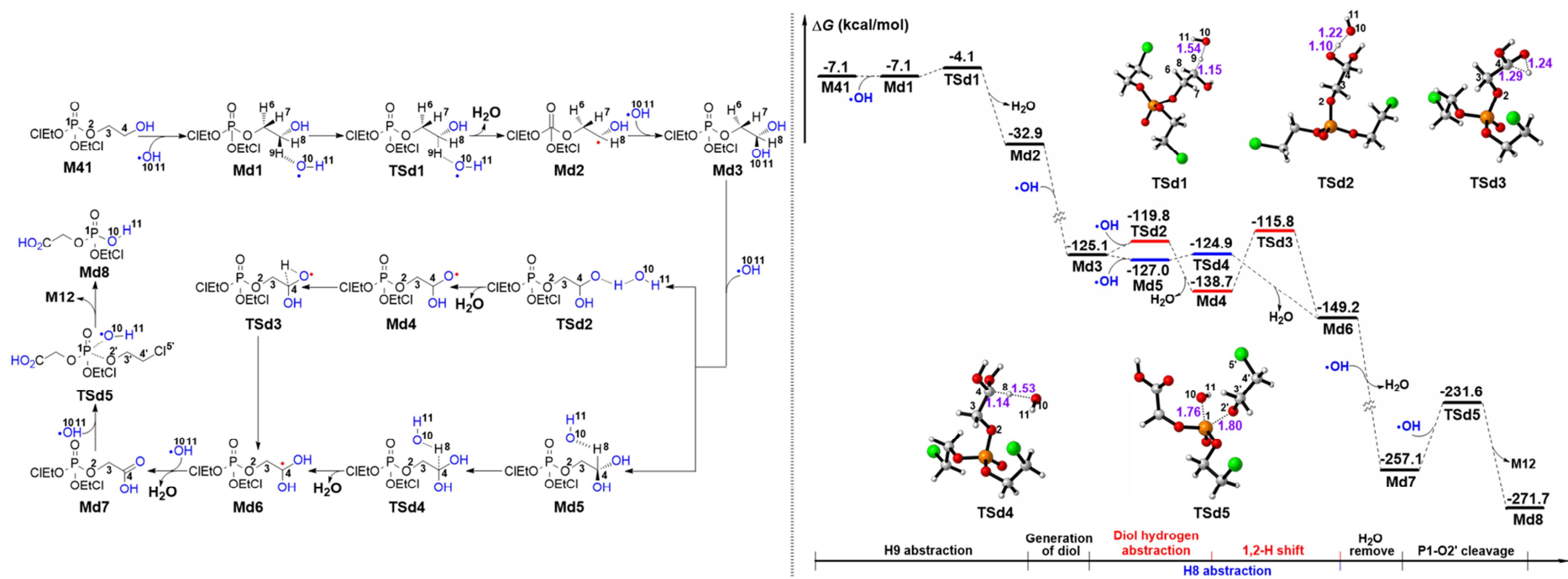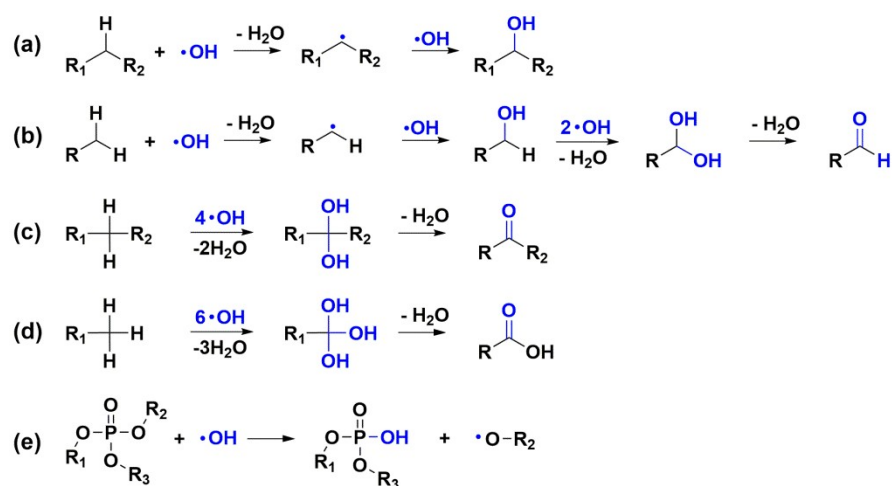
Figure 8. The possible pathways for formation of (a) alcohol, (b) aldehyde, (c) ketone, (d) carboxylic acid, and (e) phosphodiester.

4. Conclusions

By using the DFT method this work investigates the following mechanism of TCEP degradation: the H abstractions (HAP) first proceed through a prereactive complex, followed by a transition state and finally the production of the TCEP-radical along with a water molecule. All transition states are located less than 4 kcal/mol above the initial reactants, indicating the very fast processes. If the degradation undergoes the ·OH attack pathway (RAP), the carbon adjacent to the oxygen atom is revealed to be unreactive, while the barriers of attack onto the P1 atom to break the P-O bond or onto the terminal carbon atom to cleavage the C-Cl bond are both reasonable values for mild experimental conditions. In addition, the study indicates further transformation of the given intermediates by Path I and Path IV of the RAP mechanism. All the proposed conversion pathways were demonstrated to be reasonable for the experimental conditions and significantly exothermic, implying remarkable tendency of the forward reaction. The DFT approach provided an important insight on how these experimentally detected degradation products were generated. This work offers a theoretical guide for further research on the TCEP degradation, especially in the advanced oxidation processes.

Declaration of Competing Interest

The authors report no declarations of interest.

Acknowledgements

5. References

Abdullah, A.M., O'Shea, K.E., 2019. TiO2 photocatalytic degradation of the flame retardant tris (2-chloroethyl) phosphate (TCEP) in aqueous solution: A detailed kinetic and mechanistic study. J Photoch. Photobio. A 377, 130-137. http://doi.org/10.1016/j.jphotochem.2019.03.026.

Ahmad, M.A., Javed R., Adeel M., Rizwan M., Ao Q., Yang Y., 2020. Engineered ZnO and CuO Nanoparticles Ameliorate Morphological and Biochemical Response in Tissue Culture Regenerants of Candyleaf. Molecules 25, 1356. http://doi.org/10.3390/molecules25061356

Alvarez-Corena, J.R., Bergendahl, J.A., Hart, F.L., 2016. Advanced oxidation of five contaminants in water by UV/TiO2: Reaction kinetics and byproducts identification. J. Environ. Manage. 181, 544-551. http://dx.doi.org/10.1016/j.jenvman.2016.07.015.

Antonopoulou, M., Karagianni, P., Konstantinou, I.K., 2016. Kinetic and mechanistic study of photocatalytic degradation of flame retardant Tris (1-chloro-2-propyl) phosphate (TCPP). Appl. Catal. B: Environ. 192, 152-160. http://dx.doi.org/10.1016/j.apcatb.2016.03.039.

Bai, H., Xu, H., Zhang, H., Guo, Y., Shan, J., Wei, D., Zhu, Y., Zhang, S., Zhang, W., 2018. Theoretical investigations of the Ir-catalyzed direct borylation of B(3,6)–H of o-carborane: the actual catalyst, mechanism, and origin of regioselectivity. Catal. Sci. Technol. 8, 5165-5177. http://doi.org/10.1039/c8cy01322e.

Bai, H., Zhang, H., Guo, Y., Chen, H., Wei, D., Li, S., Zhu, Y., Zhang, W., 2019a. Understanding the Z selectivity of the metal-free intermolecular aminoarylation of alkynes: a DFT study. Org. Chem. Front. 6(1), 125-133. http://doi.org/10.1039/c8qo01093e.

Bai, H., Zhang, H., Zhang, X., Wang, L., Li, S., Wei, D., Zhu, Y., Zhang, W., 2019b. Unravelling the Origins of Hydroboration Chemoselectivity Inversion Using an N,O-Chelated Ir(I) Complex: A Computational Study. J. Org. Chem. 84(11), 6709-6718. http://doi.org/10.1021/acs.joc.9b00329.

Biard, P.-F., Dang, T.T., Bocanegra, J., Couvert, A., 2018. Intensification of the O3/H2O2 advanced oxidation process using a continuous tubular reactor filled with static mixers: Proof of concept. Chem. Eng. J. 344, 574-582. http://doi.org/10.1016/j.cej.2018.03.112.

Cechova, E., Vojta, S., Kukucka, P., Kocan, A., Trnovec, T., Murinova, L.P., de Cock, M., van de Bor, M., Askevold, J., Eggesbo, M., Scheringer, M., 2017. Legacy and alternative halogenated flame retardants in human milk in Europe: Implications for children's health. Environ. Int. 108, 137-145. http://dx.doi.org/10.1016/j.envint.2017.08.008.

Chai, J.-D., Head-Gordon, M., 2008. Long-range corrected hybrid density functionals with damped atom–atom dispersion corrections. Phys. Chem. Chem. Phy. 10(44), 6615-6620. http://dx.doi.org/10.1039/B810189B.

Chen, Q., Zheng, J., Xu, J., Dang, Z., Zhang, L., 2019a. Insights into sulfamethazine adsorption interfacial interaction mechanism on mesoporous cellulose biochar: Coupling DFT/FOT simulations with experiments. Chem. Eng. J. 356, 341-349. http://doi.org/10.1016/j.cej.2018.09.055.

Chen, X., Bester, K., 2009. Determination of organic micro-pollutants such as personal care products, plasticizers and flame retardants in sludge. Anal. Bioanal. Chem. 395(6), 1877-1884. http://doi.org/10.1007/s00216-009-3138-5.

Chen, Y., Ye, J., Chen, Y., Hu, H., Zhang, H., Ou, H., 2019b. Degradation kinetics, mechanism and toxicology of tris(2-chloroethyl) phosphate with 185 nm vacuum ultraviolet. Chem. Eng. J. 356, 98-106. http://doi.org/10.1016/j.cej.2018.09.007.

Cui, K., Wen, J., Zeng, F., Li, S., Zhou, X., Zeng, Z., 2017. Occurrence and distribution of organophosphate esters in urban soils of the subtropical city, Guangzhou, China. Chemosphere 175, 514-520. http://dx.doi.org/10.1016/j.chemosphere.2017.02.070.

da Silva, W.P., Carlos, T.D., Cavallini, G.S., Pereira, D.H., 2020. Peracetic acid: Structural elucidation for applications in wastewater treatment. Water Res. 168, 115143. http://doi.org/10.1016/j.watres.2019.115143.

Dill, J.D., Pople, J.A., 1975. Self-consistent molecular orbital methods. XV. Extended Gaussian-type basis sets for lithium, beryllium, and boron. J. Chem. Phys. 62(7), 2921-2923. http://dx.doi.org/10.1063/1.430801.

Du, L., Wang, X., Wu, J., 2018. Degradation of tri(2-chloroethyl)phosphate by a microwave enhanced heterogeneous Fenton process using iron oxide containing waste. RSC Adv. 8(32), 18139-18145. http://doi.org/10.1039/c8ra02911c.

24

Dzade, N.Y., Roldan, A., de Leeuw, N.H., 2017. Structures and Properties of As(OH)3 Adsorption Complexes on Hydrated Mackinawite (FeS) Surfaces: A DFT-D2 Study. Environ. Sci. Technol. 51(6), 3461-3470. http://doi.org/10.1021/acs.est.7b00107.

ECHA, 2010. Candidate list of Substance of Very High Concern for Authorization. http://echa.europa.eu/candidate-list-table.

Fang, D.-C. 2013, free of charge for academic users. THERMO, Beijing Normal University, Beijing. Follmann, W., Wober, J., 2006. Investigation of cytotoxic, genotoxic, mutagenic, and estrogenic effects of the flame retardants tris-(2-chloroethyl)-phosphate (TCEP) and tris-(2-chloropropyl)-phosphate (TCPP) in vitro. Toxicol. Lett. 161(2), 124-134. http://doi.org/10.1016/j.toxlet.2005.08.008.

Frisch, M.J., Trucks, G.W., Schlegel, H.B., Scuseria, G.E., Robb, M.A., Cheeseman, J.R., Scalmani, G., Barone, V., Mennucci, B., Petersson, G.A., Nakatsuji, H., Caricato, M., Li, X., Hratchian, H.P., Izmaylov, A.F., Bloino, J., Zheng, G., Sonnenberg, J.L., Hada, M., Ehara, M., Toyota, K., Fukuda, R., Hasegawa, J., Ishida, M., Nakajima, T., Honda, Y., Kitao, O., Nakai, H., Vreven, T., Montgomery, J.A., Jr., J.E.P., Ogliaro, F., Bearpark, M., Heyd, J.J., Brothers, E., Kudin, K.N., Staroverov, V.N., Keith, T., Kobayashi, R., Normand, J., Raghavachari, K., Rendell, A., Burant, J.C., Iyengar, S.S., Tomasi, J., Cossi, M., Rega, N., Millam, J.M., Klene, M., Knox, J.E., Cross, J.B., Bakken, V., Adamo, C., Jaramillo, J., Gomperts, R., Stratmann, R.E., Yazyev, O., Austin, A.J., Cammi, R., Pomelli, C., Ochterski, J.W., Martin, R.L., Morokuma, K., Zakrzewski, V.G., Voth, G.A., Salvador, P., Dannenberg, J.J., Dapprich, S., Daniels, A.D., Farkas, O., Foresman, J.B., Ortiz, J.V., Cioslowski, J., Fox, D.J. 2010 Gaussian 09, Revision C. 01; Gaussian, Inc., Wallingford CT.

Ghosh, S., Verma, P., Cramer, C.J., Gagliardi, L., Truhlar, D.G., 2018. Combining Wave Function Methods with Density Functional Theory for Excited States. Chem. Rev. 118(15), 7249-7292. http://doi.org/10.1021/acs.chemrev.8b00193.

Gonzalez, C., Schlegel, H.B., 1989. An improved algorithm for reaction path following. J. Chem. Phys. 90, 2154. http://doi.org/10.1063/1.456010. Gonzalez, C., Schlegel, H.B., 1990. Reaction path following in mass-weighted internal coordinates. J. Phys. Chem. 94(14), 5523-5527. http://doi.org/10.1021/j100377a021.

Greaves, A.K., Letcher, R.J., 2017. A Review of Organophosphate Esters in the Environment from Biological Effects to Distribution and Fate. Bull. Environ. Contam. Toxicol. 98(1), 2-7. http://doi.org/10.1007/s00128-016-1898-0.

He, L., Sun, X., Zhu, F., Ren, S., Wang, S., 2017. OH-initiated transformation and hydrolysis of aspirin in AOPs system: DFT and experimental studies. Sci. Total Environ. 592, 33-40. http://dx.doi.org/10.1016/j.scitotenv.2017.03.041.

Hehre, W.J., Ditchfield, R., Pople, J.A., 1972. Self—Consistent Molecular Orbital Methods. XII. Further Extensions of Gaussian—Type Basis Sets for Use in Molecular Orbital Studies of Organic Molecules. J. Chem. Phys. 56(5), 2257-2261. http://dx.doi.org/10.1063/1.1677527.

Hoffman, K., Lorenzo, A., Butt, C.M., Hammel, S.C., Henderson, B.B., Roman, S.A., Scheri, R.P., Stapleton, H.M., Sosa, J.A., 2017. Exposure to flame retardant chemicals and occurrence and severity of papillary thyroid cancer: A case-control study. Environ. Int. 107, 235-242. http://dx.doi.org/10.1016/j.envint.2017.06.021.

Huang, F., Lu, G., Zhao, L., Li, H., Wang, Z.-X., 2010. The Catalytic Role of N-Heterocyclic Carbene in a Metal-Free Conversion of Carbon Dioxide into Methanol: A Computational Mechanism Study. J. Am. Chem. Soc. 132(35), 12388-12396. http://doi.org/10.1021/ja103531z.

Ike, I.A., Karanfil, T., Cho, J., Hur, J., 2019. Oxidation byproducts from the degradation of dissolved organic matter by advanced oxidation processes – A critical review. Water Res. 164, 114929. http://doi.org/10.1016/j.watres.2019.114929.

Kim, J.W., Isobe, T., Sudaryanto, A., Malarvannan, G., Chang, K.H., Muto, M., Prudente, M., Tanabe, S., 2013. Organophosphorus flame retardants in house dust from the Philippines: occurrence and assessment of human exposure. Environ. Sci. Pollut. Res. Int. 20(2), 812-822. http://doi.org/10.1007/s11356-012-1237-x.

Kim, U.J., Oh, J.K., Kannan, K., 2017. Occurrence, Removal, and Environmental Emission of Organophosphate Flame Retardants/Plasticizers in a Wastewater Treatment Plant in New York State. Environ. Sci. Technol. 51(14), 7872-7880. http://doi.org/10.1021/acs.est.7b02035.

Legault, C.Y., Garcia, Y., Merlic, C.A., Houk, K.N., 2007. Origin of Regioselectivity in Palladium-Catalyzed Cross-Coupling Reactions of Polyhalogenated Heterocycles. J. Am. Chem. Soc. 129(42), 12664-12665. http://doi.org/10.1021/ja075785o.

Li, C., Chen, J., Xie, H.B., Zhao, Y., Xia, D., Xu, T., Li, X., Qiao, X., 2017. Effects of Atmospheric Water on .OH-initiated Oxidation of Organophosphate Flame Retardants: A DFT Investigation on TCPP. Environ. Sci. Technol. 51(9), 5043-5051. http://doi.org/10.1021/acs.est.7b00347.

Li, C., Wei, G., Chen, J., Zhao, Y., Zhang, Y.-N., Su, L., Qin, W., 2018a. Aqueous OH Radical Reaction Rate Constants for Organophosphorus Flame Retardants and Plasticizers: Experimental and Modeling Studies. Environ. Sci. Technol. 52(5), 2790-2799. http://doi.org/10.1021/acs.est.7b05429.

Li, G., Nykaza, T.V., Cooper, J.C., Ramirez, A., Luzung, M.R., Radosevich, A.T., 2020a. An Improved PIII/PV═O-Catalyzed Reductive C–N Coupling of Nitroaromatics and Boronic Acids by Mechanistic Differentiation of Rate- and Product-Determining Steps. J. Am. Chem. Soc. 142(14), 6786-6799. http://doi.org/10.1021/jacs.0c01666.

Li, H., Miao, X., Zhang, J., Du, J., Xu, S., Tang, J., Zhang, Y., 2020b. DFT studies on the reaction mechanism and kinetics of dibutyl phthalate initiated by hydroxyl and sulfate radicals: Prediction of the most reactive sites. Chem. Eng. J. 381, 122680. http://doi.org/10.1016/j.cej.2019.122680.

Li, H., Zhang, Y., Wan, J., Xiao, H., Chen, X., 2018b. Theoretical investigation on the oxidation mechanism of dibutyl phthalate by hydroxyl and sulfate radicals in the gas and aqueous phase. Chem. Eng. J. 339, 381-392. http://doi.org/10.1016/j.cej.2017.12.153.

Li, W., Guo, H., Wang, C., Zhang, Y., Cheng, X., Wang, J., Yang, B., Du, E., 2020c. ROS reevaluation for degradation of 4-chloro-3,5-dimethylphenol (PCMX) by UV and UV/persulfate processes in the water: Kinetics, mechanism, DFT studies and toxicity evolution. Chem. Eng. J. 390, 124610. http://doi.org/10.1016/j.cej.2020.124610.

Liang, Y., Liu, S., Xia, Y., Li, Y., Yu, Z.X., 2008. Mechanism, regioselectivity, and the kinetics of phosphine-catalyzed [3+2] cycloaddition reactions of allenoates and electron-deficient alkenes. Chem. Eur. J. 14(14), 4361-4373. http://doi.org/10.1002/chem.200701725|.

Liu, B., Liu, Z., Yu, P., Pan, S., Xu, Y., Sun, Y., Pan, S.Y., Yu, Y., Zheng, H., 2020. Enhanced removal of tris(2-chloroethyl) phosphate using a resin-based nanocomposite hydrated iron oxide through a Fenton-like process: Capacity evaluation and pathways. Water Res. 175, 115655. http://doi.org/10.1016/j.watres.2020.115655.

Liu, F., Zhou, K., Chen, Q., Wang, A., Chen, W., 2018a. Comparative study on the synthesis of magnetic ferrite adsorbent for the removal of Cd(II) from wastewater. Adsorpt. Sci. Technol. 36, 026361741877972. http://doi.org/10.1177/0263617418779729.

Liu, J., Ye, J., Chen, Y., Li, C., Ou, H., 2018b. UV-driven hydroxyl radical oxidation of tris(2-chloroethyl) phosphate: Intermediate products and residual toxicity. Chemosphere 190, 225-233. http://doi.org/10.1016/j.chemosphere.2017.09.111.

Liu, T., Yin, K., Liu, C., Luo, J., Crittenden, J., Zhang, W., Luo, S., He, Q., Deng, Y., Liu, H., Zhang, D., 2018c. The role of reactive oxygen species and carbonate radical in oxcarbazepine degradation via UV, UV/H2O2: Kinetics, mechanisms and toxicity evaluation. Water Res. 147, 204-213. http://doi.org/10.1016/j.watres.2018.10.007.

Liu, W., Li, Y., Liu, F., Jiang, W., Zhang, D., Liang, J., 2019. Visible-light-driven photocatalytic degradation of diclofenac by carbon quantum dots modified porous g-C3N4: Mechanisms, degradation pathway and DFT calculation. Water Res. 150, 431-441. http://doi.org/10.1016/j.watres.2018.12.001.

Luo, S., Gao, L., Wei, Z., Spinney, R., Dionysiou, D.D., Hu, W.P., Chai, L., Xiao, R., 2018. Kinetic and mechanistic aspects of hydroxyl radicalmediated degradation of naproxen and reaction intermediates. Water Res. 137, 233-241. http://doi.org/10.1016/j.watres.2018.03.002.

Lv, K., Guo, X., Wu, X., Li, Q., Ho, W., Li, M., Ye, H., Du, D., 2016. Photocatalytic selective oxidation of phenol to produce dihydroxybenzenes in a TiO2/UV system: Hydroxyl radical versus hole. Appl. Catal. B: Environ. 199, 405-411. http://doi.org/10.1016/j.apcatb.2016.06.049.

Ma, Y., Xie, Z., Lohmann, R., Mi, W., Gao, G., 2017. Organophosphate Ester Flame Retardants and Plasticizers in Ocean Sediments from the North Pacific to the Arctic Ocean. Environ. Sci. Technol. 51(7), 3809-3815. http://doi.org/10.1021/acs.est.7b00755.

Marenich, A.V., Cramer, C.J., Truhlar, D.G., 2009. Performance of SM6, SM8, and SMD on the SAMPL1 Test Set for the Prediction of Small-Molecule Solvation Free Energies. J. Phys. Chem. B 113(14), 4538-4543. http://doi.org/10.1021/jp809094y

Miklos, D.B., Remy, C., Jekel, M., Linden, K.G., Drewes, J.E., Hubner, U., 2018. Evaluation of advanced oxidation processes for water and wastewater treatment - A critical review. Water Res. 139, 118-131. http://doi.org/10.1016/j.watres.2018.03.042.

Navalon, S., Alvaro, M., Garcia, H., 2010. Heterogeneous Fenton catalysts based on clays, silicas and zeolites. Appl. Catal. B: Environ. 99(1-2), 1-26. http://doi.org/10.1016/j.apcatb.2010.07.006.

Pang, L., Yang, H., Wang, Y., Luo, X., Liu, S., Xiao, J., 2019. Organophosphate flame retardants in total suspended particulates from an urban area of zhengzhou, China: Temporal variations, potential affecting factors, and health risk assessment. Ecotoxicol. Environ. Saf. 176, 204-210. http://doi.org/10.1016/j.ecoenv.2019.03.092.

Pantelaki, I., Voutsa, D., 2019. Organophosphate flame retardants (OPFRs): A review on analytical methods and occurrence in wastewater and aquatic environment. Sci. Total Environ. 649, 247-263. http://doi.org/10.1016/j.scitotenv.2018.08.286.

Ran, Y., Tang, M., Wang, Y., Wang, Y., Zhang, X., Zhu, Y., Wei, D., Zhang, W., 2016. Theoretical investigations towards the [4+2] cycloaddition of ketenes with 1-azadienes catalyzed by N -heterocyclic carbenes: mechanism and stereoselectivity. Tetrahedron 72(35), 5295-5300. http://dx.doi.org/10.1016/j.tet.2016.06.057.

Reemtsma, T., Quintana, J.B., Rodil, R., García-López, M., Rodríguez, I., 2008. Organophosphorus flame retardants and plasticizers in water and air I. Occurrence and fate. TrAC Trend. Anal. Chem. 27(9), 727-737. http://doi.org/10.1016/j.trac.2008.07.002.

Rusevova Crincoli, K., Huling, S.G., 2020. Hydroxyl radical scavenging by solid mineral surfaces in oxidative treatment systems: Rate constants and implications. Water Res. 169,115240. http://doi.org/10.1016/j.watres.2019.115240.

Salimi, M., Esrafili, A., Gholami, M., Jonidi Jafari, A., Rezaei Kalantary, R., Farzadkia, M., Kermani, M., Sobhi, H.R., 2017. Contaminants of emerging concern: a review of new approach in AOP technologies. Environ. Monit. Assess. 189(8), 414. http://doi.org/10.1007/s10661-017-6097-x.

Song, X., Wen, Y., Wang, Y., Adeel, M., Yang, Y., 2018. Environmental risk assessment of the emerging EDCs contaminants from rural soil and aqueous sources: Analytical and modelling approaches. Chemosphere 198, 546-555. http://doi.org/10.1016/j.chemosphere.2018.01.060.

Sorensen, J.P., Lapworth, D.J., Nkhuwa, D.C., Stuart, M.E., Gooddy, D.C., Bell, R.A., Chirwa, M., Kabika, J., Liemisa, M., Chibesa, M., Pedley, S., 2015. Emerging contaminants in urban groundwater sources in Africa. Water Res. 72, 51-63. http://dx.doi.org/10.1016/j.watres.2014.08.002.

Tang, T., Lu, G., Wang, W., Wang, R., Huang, K., Qiu, Z., Tao, X., Dang, Z., 2018. Photocatalytic removal of organic phosphate esters by TiO2: Effect of inorganic ions and humic acid. Chemosphere 206, 26-32. http://doi.org/10.1016/j.chemosphere.2018.04.161.

Traverso, L., Phillips T.N., Yang Y., 2014. Efficient stochastic FEM for flow in heterogeneous porous media. Part 1: random Gaussian conductivity coefficients. Int. J. Numer. Meth. Fl. 74 (5): 359–385. https://doi.org/10.1002/fld.3854.

Vleeschouwer, F.D., Speybroeck, V.V., Waroquier, M., Geerlings, P., Proft, F.D., 2008. An Intrinsic Radical Stability Scale from the Perspective of Bond Dissociation Enthalpies: A Companion to Radical Electrophilicities. J. Org. Chem. 73(22), 9109-9120. http://doi.org/10.1021/jo802018b.

Wang, G., Cao, J., Gao, L., Chen, W., Huang, W., Cheng, X., Li, S., 2017. Metal-Free Synthesis of C-4 Substituted Pyridine Derivatives Using Pyridine-boryl Radicals via a Radical Addition/Coupling Mechanism: A Combined Computational and Experimental Study. J. Am. Chem. Soc. 139(10), 3904-3910. http://doi.org/10.1021/jacs.7b00823.

Wang, J., Chang, K., Sun, Z., Lee, J.H., Tackett, B.M., Zhang, C., Chen, J.G., Liu, C.-J., 2019. A Combined experimental and theoretical study of the accelerated hydrogen evolution kinetics over wide pH range on porous transition metal doped tungsten phosphide electrocatalysts. Appl. Catal. B: Environ. 251, 162-167. http://doi.org/10.1016/j.apcatb.2019.03.065.

Wang, Y., Jing, B., Wang, F., Wang, S., Liu, X., Ao, Z., Li, C., 2020. Mechanism Insight into enhanced photodegradation of pharmaceuticals and personal care products in natural water matrix over crystalline graphitic carbon nitrides. Water Res. 180, 115925. http://doi.org/10.1016/j.watres.2020.115925.

Wang, Y., Wei, D., Zhang, W., 2018. Recent Advances on Computational Investigations ofN-Heterocyclic Carbene Catalyzed Cycloaddition/Annulation Reactions: Mechanism and Origin of Selectivities. ChemCatChem 10(2), 338-360. http://dx.doi.org/10.1002/cctc.201701119.

Wei, G.L., Li, D.Q., Zhuo, M.N., Liao, Y.S., Xie, Z.Y., Guo, T.L., Li, J.J., Zhang, S.Y., Liang, Z.Q., 2015. Organophosphorus flame retardants and plasticizers: sources, occurrence, toxicity and human exposure. Environ. Pollut. 196, 29-46. http://dx.doi.org/10.1016/j.envpol.2014.09.012

Wen, Y.J., Yang, Y.S., Ren, H.J., Du, X.Q., Yang, X.Y., Zhang, L.Y., Wang, X.S., 2015. Chemical–biological hybrid reactive zones and their impact on biodiversity of remediation of the nitrobenzene and aniline contaminated groundwater. Chem. Eng. J. 280, 233-240. http://doi.org/10.1016/j.cej.2015.05.123.

Wolschke, H., Suhring, R., Xie, Z., Ebinghaus, R., 2015. Organophosphorus flame retardants and plasticizers in the aquatic environment: A case study of the Elbe River, Germany. Environ. Pollut. 206, 488-493. http://dx.doi.org/10.1016/j.envpol.2015.08.002.

Wu, L., Chladkova, B., Lechtenfeld, O.J., Lian, S., Schindelka, J., Herrmann, H., Richnow, H.H., 2018. Characterizing chemical transformation of organophosphorus compounds by 13C and 2H stable isotope analysis. Sci. Total Environ. 615, 20-28. http://doi.org/10.1016/j.scitotenv.2017.09.233.

Xiao, R., Gao, L., Wei, Z., Spinney, R., Luo, S., Wang, D., Dionysiou, D.D., Tang, C.J., Yang, W., 2017. Mechanistic insight into degradation of endocrine disrupting chemical by hydroxyl radical: An experimental and theoretical approach. Environ. Pollut. 231(Pt 2), 1446-1452. http://dx.doi.org/10.1016/j.envpol.2017.09.006.

Xu, X., Chen, J., Qu, R., Wang, Z., 2017. Oxidation of Tris (2-chloroethyl) phosphate in aqueous solution by UV-activated peroxymonosulfate: Kinetics, water matrix effects, degradation products and reaction pathways. Chemosphere 185, 833-843. http://dx.doi.org/10.1016/j.chemosphere.2017.07.090.

Yanai, T., Tew, D.P., Handy, N.C., 2004. A new hybrid exchange–correlation functional using the Coulomb-attenuating method (CAM-B3LYP). Chem. Phys. Lett. 393(1), 51-57. http://doi.org/10.1016/j.cplett.2004.06.011.

Yang, J., Zhao, Y., Li, M., Du, M., Li, X., Li, Y., 2019. A Review of a Class of Emerging Contaminants: The Classification, Distribution, Intensity of Consumption, Synthesis Routes, Environmental Effects and Expectation of Pollution Abatement to Organophosphate Flame Retardants (OPFRs). Int. J. Mol. Sci. 20(12). http://doi.org/10.3390/ijms20122874.

Yang, Y., Xiao, Y., Chang, Y., Cui, Y., Klobucar, G., Li, M., 2018a. Intestinal damage, neurotoxicity and biochemical responses caused by tris (2-chloroethyl) phosphate and tricresyl phosphate on earthworm. Ecotoxicol. Environ. Saf. 158, 78-86. http://doi.org/10.1016/j.ecoenv.2018.04.012.

Yang, W., Zhao, F., Fang, Y., Li, L., Li, C., Ta, N., 2018b. 1H-nuclear magnetic resonance metabolomics revealing the intrinsic relationships between neurochemical alterations and neurobehavioral and neuropathological abnormalities in rats exposed to tris(2-chloroethyl)phosphate. Chemosphere 200, 649-659. http://doi.org/10.1016/j.chemosphere.2018.02.056.

Ye, J., Liu, J., Li, C., Zhou, P., Wu, S., Ou, H., 2017. Heterogeneous photocatalysis of tris(2-chloroethyl) phosphate by UV/TiO2: Degradation products and impacts on bacterial proteome. Water Res. 124, 29-38. http://dx.doi.org/10.1016/j.watres.2017.07.034.

Zhang, H., Bai, H., Guo, Y., Wei, D., Chen, H., Zhu, Y., Zhang, W., 2019. A density functional theory study on mechanism and substituent effects of a base-free and catalyst-free synthesis of functionalized dihydrobenzoxazoles. Int. J. Quantum Chem. 119(6), e25836. http://doi.org/10.1002/qua.25836.

Zhang, X, Y Yang, Y Lu, Y Wen, P Li, G Zhang, 2018. Bioaugmented soil aquifer treatment for P-nitrophenol removal in wastewater unique for cold regions.Water Research 144 (2018) 616-627

Zhang, Y., Zhou, M., 2019. A critical review of the application of chelating agents to enable Fenton and Fenton-like reactions at high pH values. J. Hazard. Mater. 362, 436-450. http://doi.org/10.1016/j.jhazmat.2018.09.035.

Zhanqi, G., Shaogui, Y., Na, T., Cheng, S., 2007. Microwave assisted rapid and complete degradation of atrazine using TiO2 nanotube photocatalyst suspensions. J. Hazard. Mater. 145(3), 424-430. http://doi.org/10.1016/j.jhazmat.2006.11.042.

Zhao, Y., Truhlar, D.G., 2006. A new local density functional for main-group thermochemistry, transition metal bonding, thermochemical kinetics, and noncovalent interactions. J. Chem. Phys. 125(19), 194101. http://dx.doi.org/10.1063/1.2370993.

Zhou, Y., Liu, X., Jiang, W., Shu, Y., 2018. Theoretical insight into reaction mechanisms of 2,4-dinitroanisole with hydroxyl radicals for advanced oxidation processes. J. Mol. Model. 24(2), 44. http://doi.org/10.1007/s00894-018-3580-4.